바이오시스템공학(Journal of Biosystems Engineering) Vol. 29. No. 2, pp. 141~150 (2004)

연속살균장치에서의 액상/고상 식품간의 대류열전달계수 예측

Fluid/Particulate Heat Transfer Coefficient in a Continuous Flow Cooking System

최중섭 정회원 홍지향 정회원 고학균 정회원
J. S. Choe J. H. Hong H. K. Koh

적 요

우리가 소비하는 가공 식품은 위생상 안전하도록 살균처리가 이루어진다. 식품 내에 존재할 수 있는 유해 세균은 일정 살균온도에서 살균에 필요한 시간 동안 노출되면 사멸하며, 일반적으로 살균온도가 높을수록 살균에 필요한 시간은 단축된다. 연속살균장치는 혼합 및 저장탱크에 담겨진 식품을 펌프로 이동시키면서 가열 열교환기에서 살균온도로 가열하고 단열관을 거치는 동안 살균온도를 유지시켜 살균을 완료한다. 또한 살균된 식품은 냉각용 열교환기에서 상온으로 냉각되며 이 과정에서 회수되는 열은 저장탱크에서 유입되는 식품의 예열에 사용되어 에너지 효율을 제고하는데 사용되기도 한다. 이와 같이 관을 이동하면서 가열되는 살균장치는 기존의 배치식 살균방법에 비하여 균일하게 가열이 이루어지므로 130C의 고온으로 살균할 수 있어서 살균에 필요한 시간을 수초에서 수십초 정도로 단축시킬 수가 있고 그에 따라 열손상을 크게 줄일 수 있다. 또한, 상온으로 냉각된 식품을 포장함으로써 저렴한 가격의 포장용기를 사용할 수 있고 상온에서 저장할 수 있으므로 저장비용이 저렴한 장점이 있다.

그러나, 가공식품에 고기나 야채와 같은 고체 상태의 식품이 함유된 경우에는 액상 식품이 열 교환기에서 순간 가열되며, 고상 식품은 액상식품과의 대류에 의한 열전달로 가열된다. 이 과정에서 고상식품은 이동관 내벽이나 다른 고상식품과 부딪치거나 회전하면서 이동관 내부에서 자유롭게 운동하게 된다. 이 과정에서 액상식품과의 상대이동 속도가 발생하여 이것이 대류열전달에 영향을 미치게 된다. 이 상대이동속도에 따른 대류 열전달계수는 고상식품의 내부온도 결정에 사용되는 연속살균장치의 중요한 설계인자이다. 대류열전달계수는 연속살균장치에서 자유로이 이동하는 고상식품의 중심부의 온도를 측정하여 결정할 수 있으나 이는 현실적으로 어렵다. 따라서 본 연구에서는 고정된 고상식품에 액상식품을 이동시켜 상대속도를 재현하고 액상식품의 온도와 고상식품의 중심온도를 측정하는 장치를 개발하였으며, 각 상대속도와 액상식품의 점도 별 대류열전달계수를 결정하는 프로그램을 유한차분법을 이용하여 개발하였다.

이 장치를 분당 15, 30, 40 리터의 유량에서 유체의 점도를 0에서 15 centipoise 사이의 세 수준에서 청육면체 소고기를 모델 고상식품으로 내부 온도분포를 측정하였으며, 유한차분법 프로그램으로 대류열전달계수를 결정하였다. 대류열전달계수는 792에서 2,107 W/m^{2}K로 분석되었다. 대류열전달 계수는 액상식품과의 상대속도가 증가함에 따라서 증가하였고, 점도가 증가함에 따라서는 감소하였다.

Keywords : Convection, Finite Difference, Food Processing, Heat Transfer, Simulation.

1. INTRODUCTION

Aseptic processing is a method for thermal sterile processing of food products which move in a continuous flow through heat-hold-cool thermal processes and are then filled in sterile packages under sterile conditions. Due to ultra-high temperatures used in the heating process, aseptic processing requires a much shorter time as compared to traditional preparation methods such as retorting. Therefore, it has the potential to minimize damage to food

The authors are Jung Seub Choe, Associate Professor, Ji Hyang Hong, BK21 Professor, School of Mechanical Engineering, Sangju National University and Hak Kyun Koh, Professor, Department of Agricultural and Biological Engineering, Seoul National University. The corresponding author is J. S. Choe, Associate Professor, School of Mechanical Engineering, Sangju National University, 386 Gajang-dong, Sangju-city, Kyung Buk, 742-711, Korea.. E-mail : <jschoe@sangju.ac.kr>.

products, improve product quality, reduce energy consumption, and increase productivity. The continuous thermal sterilization process has been favorably used with homogeneous high acid foods as an economical and efficient means of destroying microorganisms and inactivating enzymes in foods. However, this process has not been very successful for low acid foods containing discrete particulate materials because of the problem of assuring complete sterilization.

Sterility of discrete particulate materials can be estimated by measuring temperature history of the coldest point in a particle moving through a continuous flow thermal process. To date, there is no practical method available to measure the temperature of a food particle moving through an aseptic system. In recent years, either biological methods or mathematical models have been used to estimate sterility in low-acid foods containing particulates. Biological methods rely on a count-reduction procedure of heat resistant bacterial spores in inoculated particulates. These biological methods are tedious and unreliable because they depend on undefinable conditions of aseptic processing.

Therefore, mathematical simulation models have been popular for predicting temperature profiles of moving particles to estimate accumulated lethality during aseptic processing. Mathematical simulation models depend on input parameters such as thermal properties of both fluids and particulates, convection heat transfer coefficient between fluid and particulate, and residence time in each process. Thermal properties of both particles and fluids such as specific heat and thermal conductivity can be measured experimentally. Specific heat of sample foods can be accurately measured using Differential Scanning Calorimetry(DSC) methods(Mohsenin, 1980). Thermal conductivity of both fluids and particulates can be accurately measured using a thermal probe method as reported by Hong et al.(1998).

However, many mathematical models(de Ruyter and Brunet, 1973; Manson and Cullen, 1974; Sastry, 1986) use either infinite or assumed values for convection heat transfer coefficient because of the difficulties of determining reliable values. Since convection heat transfer at the boundary between fluids and particulates can be estimated from temperature-time profiles of fluids and particulates, several apparatus have been designed to measure the center temperature-time profile of a food particulate in a fluid stream(Zuritz et al., 1987; Chandarana et al., 1988; Chang and Toledo, 1989; Alhamdan et al., 1990). Most of these studies mounted a stationary sample in a sample holder and measured particulate center temperature during continuous flow heating at a constant fluid temperature. However, the effects of thermal conduction through the sample holding frame and varying characteristics of fluid flow in a real system were not considered.

The objectives of this study were:

1) to design a dynamic thermal property evaluation system to measure temperature-time profiles of a food particulate in a continuous flow cooking system,

2) to develop a finite difference model to predict the temperature distribution of a cube particle in a continuous flow cooking system,

3) to estimate the fluid/particulate heat transfer coefficients from measured and simulated temperature-time profiles of the food particulates, and

4) to determine the effects of viscosity and flow rate of the carrier fluid on the fluid/particulate heat transfer coefficient.

2. CONTINUOUS FLOW COOKING SYSTEM

An experimental apparatus developed by Black(1994) was modified to simulate a continuous flow cooking system as shown in Fig. 1. The modifications consisted of an improved mixing tank, custom flow meter, sample holder, and a sample introducing device. A 250liter stainless steel mixing tank was thermally insulated with 5cm thick glass wool and a 5.08cm I.D. drainpipe was attached at the bottom. A custom flow meter was installed between the

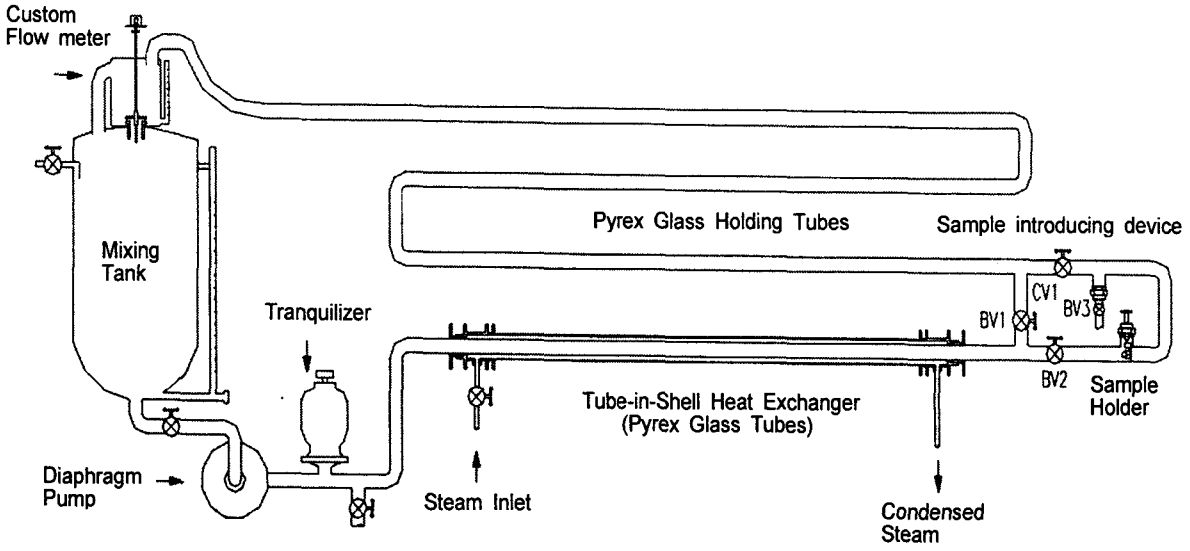

Fig. 1 Schematic diagram of the continuous flow cooking system.

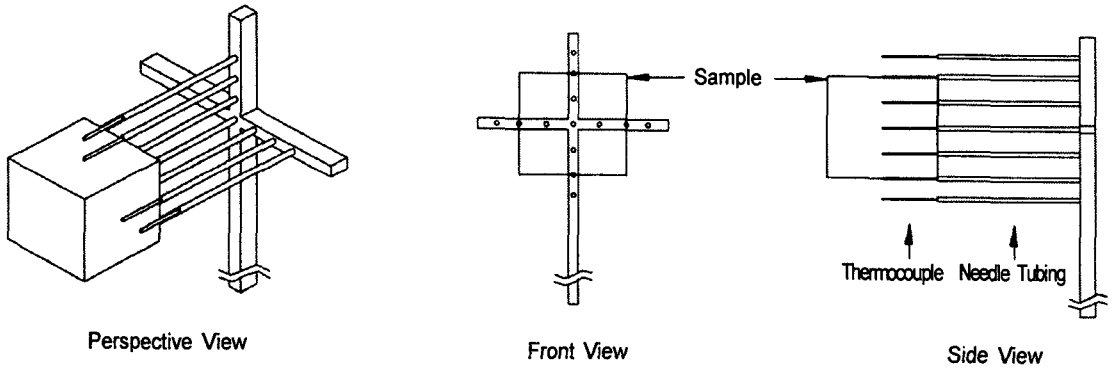

Fig. 2 Schematics of the sample holder and thermocouple locations.

third holding-tube section and the mixing tank. It consisted of a 20 liter bucket, baffle tube, fluid level sensors, and a disk valve at the bottom of the bucket, which was driven by a solenoid on the top of the bucket. A control circuit board and 1.0 millisecond clock pulse generator were designed to control the flow rate measurement. Infrared photo devices were installed on the fluid level indicating tube and used as fluid level sensors. Fluid flow rate was determined by measuring the time required to fill an 11.3-liter volume between the two upper fluid level sensors.

Fig. 2 shows a sample holder which was designed to place a sample in the center of the flow tube while minimizing flow disturbance and heat transfer through the sample holder frame. Brass material was formed into a cross-shaped frame of 2.0 ± 0.05mm wide and 3.0 ± 0.05mm thick and thirteen stainless steel needle tubes (20gage Type 304 stainless steel #3 temper, Popper and Sons Inc.) were mounted through the brass frame. Teflon insulated 40 gauge type-T thermocouples (Physitemp Instrument Inc., NJ) were installed through the stainless steel needle tubes so that the tip of each thermocouple protruded 7.5mm from the end of each stainless steel tube. A sample preparation device was designed to make all particulate samples to the exact same size and shape and to make indentations inside a sample for thermocouples.

The sample was placed over the thermocouples so that only the ends of the needle tubes were in contact with the surface of the sample to minimize thermal conduction from the frame to the sample. Five thermocouples were placed inside the sample to measure temperatures at the center and four intermediate points. Eight other thermocouples were used to measure fluid temperature profiles at the sample surface and around the sample. All thermocouples were spaced 3.75mm apart.

A sample-introducing device was designed to bypass fluid flow from the sample mounting area and was placed between the heat exchanger and holding tube section. Fig. 3 shows the sample holder mounted in a brass coupling adapter in a glass T-tube section with a quick coupling device. During heating of a meat cube in the continuous flow cooking system, the flow pattern was observed through the glass-T where sample holder was placed. Since the sample was placed in front of the sample holder in fluid steam as shown in Fig. 3, no pronounced flow disturbance was observed around the sample holder.

Temperature profiles inside the sample and fluid around the sample were measured every 2 seconds with a CR7X measurement and control system(Campbell Scientific, Inc., UT). The data logger was interfaced to an IBM-PC compatible microcomputer through an RS-232 port for real-time display and permanent storage of temperature-time-profiles and flow rates.

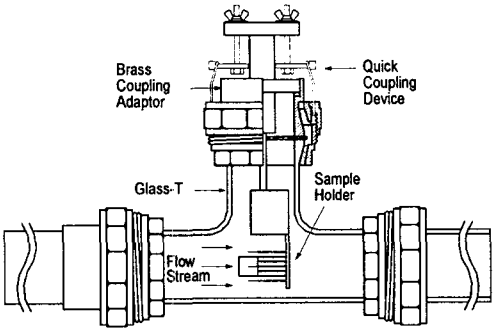

Fig. 3 Schematic of the quick coupling device for the sample holder.

A. A Finite Difference Model

A finite difference model was developed to predict temperature distributions inside a meat cube in a continuous flow cooking system. Since flow patterns are different at the front surface, side surfaces, and backside of a cube with respect to flow direction, convection heat transfer rate on each side of the cube will also be different. However, since an average value of the heat transfer through all of the surfaces is the value of interest for engineers in thermal process design, heat transfer rates through all sides of the cube were assumed identical. The model cube was divided into eight identical cubes as mirror images of each other to minimize the computing time. Because of similarities, three-dimensional finite difference equations were derived using energy balances on only four different types of control volumes(inside, side, edge, and corner) as shown in Fig. 4. A mirror image cube was divided into

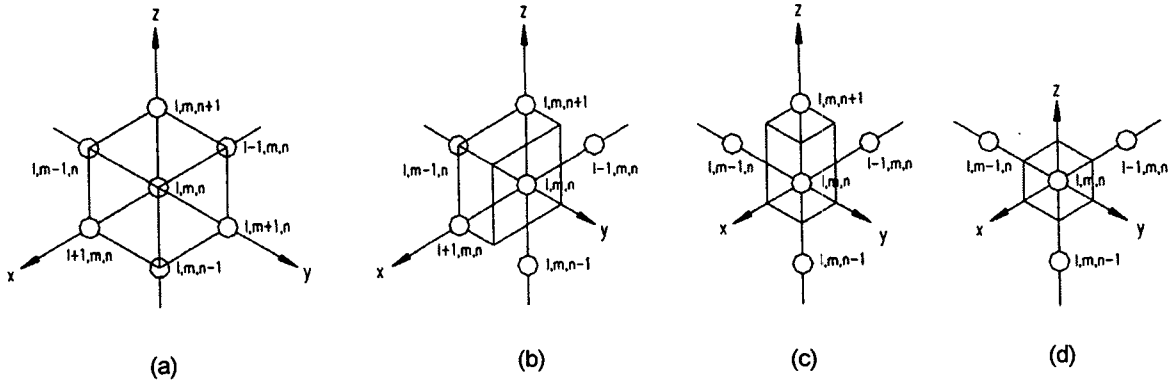

Fig. 4 Control volumes for finite difference equations.

nine by nine by nine nodes for a total of 729 nodes with 0.83mm nodal spacing.

Finite difference equations can be derived in either explicit or implicit form. For explicit methods, the stability of finite difference equations depends on the Fourier number, *Fo*:

$$Fo = \frac{k}{\rho C_p}\frac{\Delta\tau}{(\Delta x)^2} \quad \cdots\cdots (1)$$

Where k, ρ, C_p, $\Delta\tau$, and $\Delta\chi$ denote thermal conductivity, density, specific heat, time step, and nodal size, respectively. For given values of k, ρ, C_p and $\Delta\chi$, the stability of finite difference equations can be controlled by time step size. However, since k and C_p were functions of temperature in this study, it was hard to choose a time step size to assure stability for all conditions.

Implicit solution methods have an advantage of being stable for any $\Delta\tau$. However, these methods involve large truncation error at every time step, although it can be minimized by choosing small $\Delta\tau$. Among implicit solution methods, a Crank-Nicolson method gives the least accumulated truncation error(Croft and Lilley, 1977). Since the finite difference equations in this study used input parameters k and C_p as functions of temperature, the Crank-Nicolson method was employed to develop stable finite difference equations.

For nodes inside a cube, the finite difference equation based on the control volume shown in Fig. 4-(a) is:

$$\begin{aligned}&\rho C_p \Delta x\Delta y\Delta z\frac{(T_{l,m,n}^{p+1}-T_{l,m,n}^{p})}{\Delta\tau}\\ &= k_{x+}\Delta y\Delta z\frac{(T_{l+1,m,n}^{p}-T_{l,m,n}^{p})}{\Delta x}+k_{x-}\Delta y\Delta z\frac{(T_{l-1,m,n}^{p}-T_{l,m,n}^{p})}{\Delta x}\\ &+ k_{y+}\Delta z\Delta x\frac{(T_{l,m+1,n}^{p}-T_{l,m,n}^{p})}{\Delta y}+k_{y-}\Delta z\Delta x\frac{(T_{l,m-1,n}^{p}-T_{l,m,n}^{p})}{\Delta y}\\ &+ k_{z+}\Delta x\Delta y\frac{(T_{l,m,n+1}^{p}-T_{l,m,n}^{p})}{\Delta z}+k_{z-}\Delta x\Delta y\frac{(T_{l,m,n-1}^{p}-T_{l,m,n}^{p})}{\Delta z}\end{aligned} \quad \cdots\cdots (2)$$

Where ρ, C_p, $\Delta\tau$, $T^{p+1}{}_{l,m,n}$, and $T^{p}{}_{l,m,n}$ denote the density, specific heat, time step, temperatures at times $p+1$ and p at location(l,m,n), respectively. Since $\Delta\chi = \Delta y = \Delta z$ and by setting $\zeta = C_p(\Delta\chi)^2/\Delta\tau$, Equation(2) becomes:

$$\begin{aligned}&\zeta(T_{l,m,n}^{p+1}-T_{l,m,n}^{p})\\ &= k_{x+}(T_{l+1,m,n}^{p}-T_{l,m,n}^{p})+k_{x-}(T_{l-1,m,n}^{p}-T_{l,m,n}^{p})+k_{y+}(T_{l,m+1,n}^{p}-T_{l,m,n}^{p})\\ &+ k_{y-}(T_{l,m-1,n}^{p}-T_{l,m,n}^{p})+k_{z+}(T_{l,m,n+1}^{p}-T_{l,m,n}^{p})+k_{z-}(T_{l,m,n-1}^{p}-T_{l,m,n}^{p})\end{aligned} \quad \cdots\cdots (3)$$

Using Crank-Nicolson methods, Equation (3) becomes:

$$\begin{aligned}&\zeta(T_{l,m,n}^{p+1}-T_{l,m,n}^{p})\\ &= 0.5\times[k_{x+}(T_{l+1,m,n}^{p}-T_{l,m,n}^{p})+k_{x-}(T_{l-1,m,n}^{p}-T_{l,m,n}^{p})\\ &+k_{y+}(T_{l,m+1,n}^{p}-T_{l,m,n}^{p})+k_{y-}(T_{l,m-1,n}^{p}-T_{l,m,n}^{p})\\ &+k_{z+}(T_{l,m,n+1}^{p}-T_{l,m,n}^{p})+k_{z-}(T_{l,m,n-1}^{p}-T_{l,m,n}^{p})]\\ &+ 0.5\times[k_{x+}(T_{l+1,m,n}^{p+1}-T_{l,m,n}^{p+1})+k_{x-}(T_{l-1,m,n}^{p+1}-T_{l,m,n}^{p+1})\\ &+k_{y+}(T_{l,m+1,n}^{p+1}-T_{l,m,n}^{p+1})+k_{y-}(T_{l,m-1,n}^{p+1}-T_{l,m,n}^{p+1})\\ &+k_{z+}(T_{l,m,n+1}^{p+1}-T_{l,m,n}^{p+1})+k_{z-}(T_{l,m,n-1}^{p+1}-T_{l,m,n}^{p+1})]\end{aligned} \quad \cdots\cdots (4)$$

Where ζ was calculated for the C_p value at temperature $T^{p}{}_{l,m,n}$ and k_x+ was the k value for the average temperature of $T_{l+l,m,n}$ and $T_{l,m,n}$. Values of k_x, k_y, and k_z were calculated in a similar way.

For nodes along a side of the model cube, an energy balance based on the control volume shown in Fig. 4-(b) is:

$$\begin{aligned}&\rho C_p\frac{\Delta x}{2}\Delta y\Delta z\frac{(T_{l,m,n}^{p+1}-T_{l,m,n}^{p})}{\Delta\tau}\\ &= h\Delta y\Delta z(T_f^{p}-T_{l,m,n}^{p})+k_{x-}\Delta y\Delta z\frac{(T_{l-1,m,n}^{p}-T_{l,m,n}^{p})}{\Delta x}\\ &+k_{y+}\Delta z\frac{\Delta x}{2}\frac{(T_{l,m+1,n}^{p}-T_{l,m,n}^{p})}{\Delta y}+k_{y-}\Delta z\frac{\Delta x}{2}\frac{(T_{l,m-1,n}^{p}-T_{l,m,n}^{p})}{\Delta y}\\ &+k_{z+}\frac{\Delta x}{2}\Delta y\frac{(T_{l,m,n+1}^{p}-T_{l,m,n}^{p})}{\Delta z}+k_{z-}\frac{\Delta x}{2}\Delta y\frac{(T_{l,m,n-1}^{p}-T_{l,m,n}^{p})}{\Delta z}\end{aligned} \quad \cdots\cdots (5)$$

Where h and $T_f{}^{p}$ denote fluid/particulate heat transfer coefficient and fluid temperature at time p, respectively. Since $\Delta\chi = \Delta y = \Delta z$, and by setting $\zeta = \rho C_p(\Delta\chi)^2/$ and $\beta = h\Delta\chi$, Equation(5) becomes:

$$\begin{aligned}\zeta(T_{l,m,n}^{p+1}-T_{l,m,n}^{p}) &= 2\beta(T_f^{p}-T_{l,m,n}^{p})+2k_{x-}(T_{l-1,m,n}^{p}-T_{l,m,n}^{p})\\ &+ k_{y+}(T_{l,m+1,n}^{p}-T_{l,m,n}^{p})+k_{y-}(T_{l,m-1,n}^{p}-T_{l,m,n}^{p})\\ &+ k_{z+}(T_{l,m,n+1}^{p}-T_{l,m,n}^{p})+k_{z-}(T_{l,m,n-1}^{p}-T_{l,m,n}^{p})\end{aligned} \quad \cdots\cdots (6)$$

Using Crank-Nicolson methods, Equation (6) becomes:

$$\zeta(T_{l,m,n}^{p+1}-T_{l,m,n}^{p})$$
$$=0.5\times[2\beta(T_f^p-T_{l,m,n}^p)+2k_{x-}(T_{l-1,m,n}^p-T_{l,m,n}^p)$$
$$+k_{y+}(T_{l,m+1,n}^p-T_{l,m,n}^p)+k_{y-}(T_{l,m-1,n}^p-T_{l,m,n}^p)$$
$$+k_{z+}(T_{l,m,n+1}^p-T_{l,m,n}^p)+k_{z-}(T_{l,m,n-1}^p-T_{l,m,n}^p)]$$
$$+0.5\times[2\beta(T_f^p-T_{l,m,n}^{p+1})+2k_{x-}(T_{l-1,m,n}^{p+1}-T_{l,m,n}^{p+1})$$
$$+k_{y+}(T_{l,m+1,n}^{p+1}-T_{l,m,n}^{p+1})+k_{y-}(T_{l,m-1,n}^{p+1}-T_{l,m,n}^{p+1})$$
$$+k_{z+}(T_{l,m,n+1}^{p+1}-T_{l,m,n}^{p+1})+k_{z-}(T_{l,m,n-1}^{p+1}-T_{l,m,n}^{p+1})]\cdots\cdots(7)$$

For nodes at the edge of the model cube, an energy balance based on the control volume shown in Fig. 4-(c) is:

$$\rho C_p\frac{\Delta x}{2}\frac{\Delta y}{2}\Delta z\frac{(T_{l,m,n}^{p+1}-T_{l,m,n}^{p})}{\Delta\tau}$$
$$=h\frac{\Delta y}{2}\Delta z(T_f^p-T_{l,m,n}^p)+k_{x-}\frac{\Delta y}{2}\Delta z\frac{(T_{l-1,m,n}^p-T_{l,m,n}^p)}{\Delta x}$$
$$+h\Delta z\frac{\Delta x}{2}(T_f^p-T_{l,m,n}^p)+k_{y-}\Delta z\frac{\Delta x}{2}\frac{(T_{l,m-1,n}^p-T_{l,m,n}^p)}{\Delta y}$$
$$+k_{z+}\frac{\Delta x}{2}\frac{\Delta y}{2}\frac{(T_{l,m,n+1}^p-T_{l,m,n}^p)}{\Delta z}+k_{z-}\frac{\Delta x}{2}\frac{\Delta y}{2}\frac{(T_{l,m,n-1}^p-T_{l,m,n}^p)}{\Delta z}$$
$$\cdots\cdots(8)$$

Since $\Delta\chi=\Delta y=\Delta z$, and by setting $\zeta=\rho C_p(\Delta\chi)^2/\Delta\tau$ and $\beta=h\Delta\chi$, Equation (8) becomes:

$$\zeta(T_{l,m,n}^{p+1}-T_{l,m,n}^{p})=2\beta(T_f^p-T_{l,m,n}^p)+2k_{x-}(T_{l-1,m,n}^p-T_{l,m,n}^p)$$
$$+2\beta(T_f^p-T_{l,m,n}^p)+2k_{y-}(T_{l,m-1,n}^p-T_{l,m,n}^p)$$
$$+k_{z+}(T_{l,m,n+1}^p-T_{l,m,n}^p)+k_{z-}(T_{l,m,n-1}^p-T_{l,m,n}^p)$$
$$\cdots\cdots(9)$$

Using Crank-Nicolson methods, Equation (9) becomes:

$$\zeta(T_{l,m,n}^{p+1}-T_{l,m,n}^{p})$$
$$=0.5\times[2\beta(T_f^p-T_{l,m,n}^p)+2k_{x-}(T_{l-1,m,n}^p-T_{l,m,n}^p)$$
$$+2\beta(T_f^p-T_{l,m,n}^p)+2k_{y-}(T_{l,m-1,n}^p-T_{l,m,n}^p)$$
$$+k_{z+}(T_{l,m,n+1}^p-T_{l,m,n}^p)+k_{z-}(T_{l,m,n-1}^p-T_{l,m,n}^p)]$$
$$+0.5\times[2\beta(T_f^p-T_{l,m,n}^{p+1})+2k_{x-}(T_{l-1,m,n}^{p+1}-T_{l,m,n}^{p+1})$$
$$+2\beta(T_f^p-T_{l,m,n}^{p+1})+2k_{y-}(T_{l,m-1,n}^{p+1}-T_{l,m,n}^{p+1})$$
$$+k_{z+}(T_{l,m,n+1}^{p+1}-T_{l,m,n}^{p+1})+k_{z-}(T_{l,m,n-1}^{p+1}-T_{l,m,n}^{p+1})]\cdots\cdots(10)$$

For nodes at the corner of the model cube, an energy balance based on the control volume shown in Fig. 4-(d) is:

$$\rho C_p\frac{\Delta x}{2}\frac{\Delta y}{2}\frac{\Delta z}{2}\frac{(T_{l,m,n}^{p+1}-T_{l,m,n}^{p})}{\Delta\tau}$$
$$=h\frac{\Delta y}{2}\frac{\Delta z}{2}(T_f^p-T_{l,m,n}^p)+k_{x-}\frac{\Delta y}{2}\frac{\Delta z}{2}\frac{(T_{l-1,m,n}^p-T_{l,m,n}^p)}{\Delta x}$$
$$+h\frac{\Delta z}{2}\frac{\Delta x}{2}(T_f^p-T_{l,m,n}^p)+k_{y-}\frac{\Delta z}{2}\frac{\Delta x}{2}\frac{(T_{l,m-1,n}^p-T_{l,m,n}^p)}{\Delta y}$$
$$+h\frac{\Delta x}{2}\frac{\Delta y}{2}(T_f^p-T_{l,m,n}^p)+k_{z-}\frac{\Delta x}{2}\frac{\Delta y}{2}\frac{(T_{l,m,n-1}^p-T_{l,m,n}^p)}{\Delta z}$$
$$\cdots\cdots(11)$$

Since $\Delta\chi=\Delta y=\Delta z$ and by setting $\zeta=\rho C_p(\Delta\chi)^2/\Delta\tau$ and $\beta=h\Delta\chi$, Equation (11) becomes:

$$\zeta(T_{l,m,n}^{p+1}-T_{l,m,n}^{p})=2\beta(T_f^p-T_{l,m,n}^p)+2k_{x-}(T_{l-1,m,n}^p-T_{l,m,n}^p)$$
$$+2\beta(T_f^p-T_{l,m,n}^p)+2k_{y-}(T_{l,m-1,n}^p-T_{l,m,n}^p)$$
$$+2\beta(T_f^p-T_{l,m,n}^p)+2k_{z-}(T_{l,m,n-1}^p-T_{l,m,n}^p)$$
$$\cdots\cdots(12)$$

Using Crank-Nicolson method, Equation (12) becomes:

$$\zeta(T_{l,m,n}^{p+1}-T_{l,m,n}^{p})$$
$$=0.5\times[2\beta(T_f^p-T_{l,m,n}^p)+2k_{x-}(T_{l-1,m,n}^p-T_{l,m,n}^p)+$$
$$+2\beta(T_f^p-T_{l,m,n}^p)+2k_{y-}(T_{l,m-1,n}^p-T_{l,m,n}^p)$$
$$+2\beta(T_f^p-T_{l,m,n}^p)+2k_{z-}(T_{l,m,n-1}^p-T_{l,m,n}^p)]$$
$$+0.5\times[2\beta(T_f^p-T_{l,m,n}^{p+1})+2k_{x-}(T_{l-1,m,n}^{p+1}-T_{l,m,n}^{p+1})$$
$$+2\beta(T_f^p-T_{l,m,n}^{p+1})+2k_{y-}(T_{l,m-1,n}^{p+1}-T_{l,m,n}^{p+1})$$
$$+2\beta(T_f^p-T_{l,m,n}^{p+1})+2k_{z-}(T_{l,m,n-1}^{p+1}-T_{l,m,n}^{p+1})]\cdots\cdots(13)$$

Finite difference equations (4), (7), (10), and (13) were programmed in C++ programming language(Borland International, Inc., CA).

3. FLUID/PARTICULATE HEAT TRANSFER COEFFICIENT

To estimate the effects of viscosity and flow rate of the carrier fluid on the fluid/particulate heat transfer coefficient h_{fp}, temperature-time profiles of a meat cube were mea-

sured at three levels of flow rate and for three levels of fluid viscosity. At each level of flow rate and viscosity, temperature-time profiles of six samples were measured. The effect of flow rate and viscosity levels on h_{fp} were tested using General Linear Model Procedures(GLM) of SAS(SAS, 1990).

Water, 1% CMC solutions, and 2% CMC solutions were used as the three viscosity levels, and flow rates were around 15, 30, and 45liter/min. The CMC solutions were prepared by mixing CMC(Carboxymethyl Cellulose Sodium High viscosity, Sigma Chemical Company, MO) powder with 80℃ tap water in the continuous flow cooking system. Viscosity of the 1% and 2% CMC solutions were measured at 80℃ using a Wells-Brookfield Cone/Plate Viscometer (Brookfield Engineering Lab., Inc., MA) with an 0.8° cone spindle, and were 8.4 ± 0.66 and 15.0 ± 0.21 centipoise, respectively. Carrier fluid temperature at the sample location was maintained around 80℃ and changed less than ±1℃ during any temperature-time profile measurement cycle.

Thermal properties of intact meat samples depend on the direction of muscle grain to the heat flux. Hill et al. (1967) found that k values were 8 to 16 percent higher when measured parallel to the fiber in comparison to those evaluated perpendicular to the muscle fiber grain of beef. To simplify thermal property determination, a beef frankfurter was chosen for testing due to its structural homogeneity. Oscar Mayer® brand Beef Franks were obtained from a local grocery store and used as the test material. Mean moisture content and density of these beef frankfurters were 53.7 ± 0.44%(wet basis) and 1033 ± 20kg/m^3, respectively. Moisture content was determined using a convection oven method at 75℃ for 24 hours and density was determined using a graduate cylinder and a balance. Specific heat of the beef meat was measured continuously from 10℃ to 100℃ by one degree increments using a Differential Scanning Calorimetry(DSC 2920, TA instrument, Co, NJ). Specific heat of the beef frankfurters ranged between 2729kJ/kg · K at 20℃ and 3567kJ/kg · K at 42℃. Thermal conductivity of the meat samples was measured using an instrument developed by Hong et al.(1998) over a temperature range of 20℃ to 80℃ and ranged between 0.389 to 0.350W/m · K.

To estimate h_{fp}, the temperature distribution inside a cube was computed from an initial guess value of h_{fp} until an objective function $J(h_{fp})$ was minimized. The objective function $J(h_{fp})$ was defined as the standardized sum of squares of the difference between the calculated center temperature, $T_{cal}(0,0,0,t_n)$ and its corresponding measured center temperature, $T_{exp}(0,0,0,t_n)$:

$$J(h_{fp}) = \frac{1}{N}\sum_{n=1}^{N}\left[T_{cal}(0,0,0,t_n) - T_{exp}(0,0,0,t_n)\right]^2 \cdots\cdots (14)$$

where N denotes the number of data points used in the calculations.

To find the minimum value of $J(h_{fp})$, an initial value of $J(h_{fp})$ was computed from the initial value of h_{fp}. The h_{fp} was then increased by an initial step size of Δh_{fp}, and a new value of $J(h_{fp})$ was computed for the new h_{fp}. If the value of $J(h_{fp})$ decreased, the value of h_{fp} was again increased by Δh_{fp}. If $J(h_{fp})$ increased, Δh_{fp} was multiplied by - 0.5 and the above procedure was repeated until the absolute value of $\Delta J(h_{fp})$ becomes less than 1.0E - 06. The value of h_{fp} that resulted was presented as the estimated fluid/particulate convection heat transfer coefficient for the specific experimental setup.

4. RESULTS AND DISCUSSION

Fig. 5 shows the measured center temperature-time profile of a meat cube in water, compared with simulated center temperature profiles of the cube for h_{fp} values of 200, 400, 600, 1687, and 10000W/m^2 · K. It was observed that fluid temperatures at the sample location reached steady state within 10 seconds. As the h_{fp} value increased, simulated center temperature profiles approached the measured center temperature profile. For h_{fp} values greater than 1687W/m^2 · K, the simulated temperature rise was

faster than the measured one. Simulated center temperatures showed the best match with measured temperatures when a h_{fp} value of 1687W/m^2 · K was used, which resulted in the minimum $J(h_{fp})$ value in Equation(14). $J(h_{fp})$ values increased for larger values of h_{fp} but at a much slower rate, which indicates the temperature rise at the center points depends more on thermal properties of the solid particulate than the h_{fp} value in this range as surface temperature approaches fluid temperature. Measured and simulated temperature profiles at the middle point between the surface and the center also showed a close match for this minimum $J(h_{fp})$ value as shown in Fig. 6.

Estimated mean h_{fp} values ranged from 792 to 2107 W/m^2 · K for beef frankfurter meat cubes over the three levels of flow rate and three levels of fluid viscosity as shown in Table 1.

Table 1 Mean fluid/particulate heat transfer coefficients at various flow rates and in various concentrations of CMC solution

Carrier Fluid	Heat transfer coefficient ± Standard Deviation(W/m^2 · K)		
	Low Flow Rate	Medium Flow Rate	High Flow Rate
Water	1,333 ± 137	2,107 ± 691	1,704 ± 485
1% CMC	841 ± 111	1,131 ± 273	1,273 ± 273
2% CMC	792 ± 120	1,060 ± 392	1,132 ± 220

The statistical analysis showed that fluid/particulate heat transfer coefficient was significantly influenced by flow rate and viscosity level. Estimated h_{fp} values decreased as viscosity increased, while estimated h_{fp} values increased with increases in flow rate in the 1% and 2% CMC solutions. The estimated h_{fp} values in water showed larger variations than those in CMC solutions, which was considered to be the effect of greater fluctuations in flow rates as shown in Table 2.

To check dimensional changes of meat cubes during the

Table 2. Average flow rates of carrier fluids

Carrier Fluid	Flow Rate ± Standard Deviation(liter/min)		
	Low Flow Rate	Medium Flow Rate	High Flow Rate
Water	15.6 ± 0.59	29.7 ± 0.64	45.0 ± 0.63
1% CMC	17.3 ± 0.34	30.3 ± 0.19	44.9 ± 0.12
2% CMC	18.3 ± 0.26	29.2 ± 0.18	45.2 ± 0.26

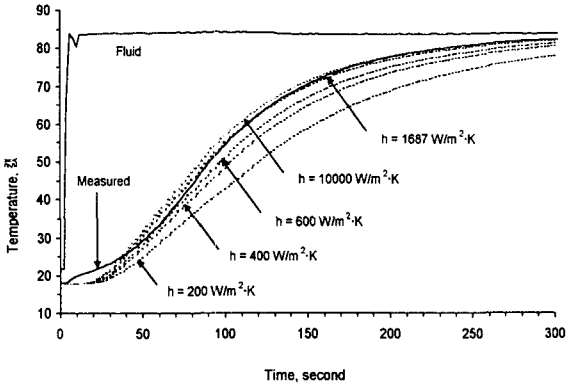

Fig. 5 Simulated and measured center temperature-time profiles of a meat cube in water at a flow rate of 14.5 liter/min.

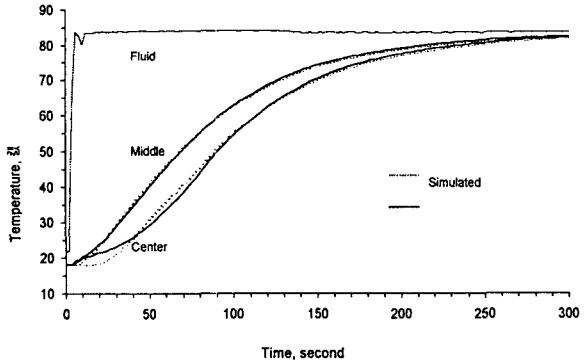

Fig. 6 Simulated and measured temperature-time profiles of the center and middle points of a meat cube for h_{fp} value of 1687 W/m^2 · K.

experimental tests, x, y, and z dimensions of the samples were measured before and after the temperature-time measurement cycle. It was found that during the tests, one of the dimensions increased as much as 13 percent while the other two decreased as much as five percent. As can

be seen in Fig. 6, measured temperatures rose faster than simulated temperatures for the first 10 seconds from the start of heating. Since the shortest path between the surface and the center point determines heating rate of a particulate, dimensional changes of meat cubes could have caused the faster rise in measured temperature. After the first 10 seconds, the measured temperature profile showed a similar shape to that of the simulated center temperatures. This was considered to indicate that no more pronounced dimensional changes occurred after the first 10 seconds. Due to the dimensional changes, a larger h_{fp} value was required in the finite difference model to make its prediction follow the actual center temperature-time profile. Therefore, h_{fp} values presented in this study could have been overestimated.

5. CONCLUSIONS

A dynamic thermal property evaluation system was designed to monitor temperature-time profiles of food particulates in a continuous flow system. The designed system was able to measure temperature-time profiles inside a meat cube and of surrounding fluid with minimum flow disturbance by the sample holder. The finite difference model was able to predict temperature distributions inside a meat cube mounted in a continuous flow cooking system. The temperature-time profiles were used effectively to estimate fluid/particulate convection heat transfer coefficient.

Estimated mean h_{fp} values ranged from 792 to 2107 $W/m^2 \cdot K$ for fluid flow rates 15.6 to 45.2liter/min and viscosity from 0 to 15.0 centipoise. As viscosity increased, the fluid/particulate heat transfer coefficient decreased. Convection heat transfer coefficient around the meat cubes increased as flow rates of 1% and 2% CMC solution increased. Due to dimensional change of samples, the h_{fp} values presented in this study could have been overestimated.

REFERENCES

1. Alhamdan, A., S. K. Sastry and J. L. Blaisdell. 1990. Natural convection heat transfer between water an irregular shaped particle. Transactions of the ASAE 33(2):620-624.
2. Black, D. G. 1994. Kinematics of elongated solid particles in viscous fluids. Unpublished Master's Thesis. Clemson University, Clemson, SC 29634.
3. Chandarana, D. I., A. Gavin, III and F. W. Wheaton. 1988. Particle/fluid interface heat transfer during aseptic processing of foods. ASAE Paper No. 88-6599. ASAE, 2950 Niles Rd., St. Joseph, MI 49085-9659.
4. Chang, S. Y. and R. T. Toledo. 1989. Heat transfer and simulated sterilization of particulate solids in a continuously flowing system. Journal of Food Science 54(4):1017-1023, 1030.
5. Croft, D. R. and D. G. Lilley. 1977. Heat transfer calculations using finite difference equations. Applied Science Publishers, LTD, London. pp. 185-187.
6. de Ruyter, P. W. and R. Brunet. 1973. Estimation of process conditions for continuous sterilization of foods containing particles. Food Technol. 27(7):44-51.
7. Hill, J. E., J. D. Leitman and J. E. Sunderland. 1967. Thermal conductivity of various meats. Food Technol. 21:1143-1148.
8. Hong, J., Y. J. Han and J. M. Bunn. 1998. Measurements of thermal conductivity of food products using a thermal probe method. ASAE Paper No. 98-6001. ASAE, 2950 Niles Rd., St. Joseph, MI 49085-9659.
9. Manson, J. E. and J. F. Cullen. 1974. Thermal process simulation for aseptic processing of food containing discrete particulate matter. Journal of Food Science 39:1084-1089.
10. Mohsenin, N. N. 1980. Thermal properties of foods and agricultural materials. Gordon and Breach Science Publishers, New York, NY.
11. SAS. 1990. SAS/STAT User's Guide, Version 6, Fourth Edition. Statistical Analysis System Institute Inc., Cary, NC.

12. Sastry, S. K. 1986. Mathematical evaluation of process schedules for aseptic processing of food containing discrete particulate matter. Journal of Food Science 51(5):1323-1328.

13. Zuritz, C. A., S. McCoy and S. K. Sastry. 1987. Convective heat transfer coefficients for non-Newtonian flow past food shaped particulates. ASAE Paper No. 87-6538. ASAE, 2950 Niles Rd., St. Joseph, MI 49085-9659.